ACS APPLIED POLYMER MATERIALS

Article

Cite This: ACS Appl. Polym. Mater. 2019, 1, 145−151

pubs.acs.org/acsapm

Sandwiched Polyethylene Shrink Film Masking with Tunable Resolution and Shape for Liquid Alloy Patterning

Bei Wang,[†,‡,⊥] Wenci Xin,[†,⊥] Klas Hjort,[‡] Chuanfei Guo,[§] and Zhigang Wu*[,†,‡]

[†]State Key Laboratory of Digital Manufacturing Equipment and Technology, Huazhong University of Science and Technology, Wuhan 430074, P. R. China

[‡]Department of Engineering Sciences, Uppsala University, Uppsala 75121, Sweden

[§]Department of Material Science and Engineering, Southern University of Science and Technology, Shenzhen 518055, P. R. China

Supporting Information

ABSTRACT: Among numerous patterning techniques, masked liquid alloy printing is one of the most promising techniques for scalable fabrication of liquid-alloy-based stretchable electronics. Like any other mask-based process, its resolution is often constrained by the quality of the mask, and the fabrication cost increases drastically with increased resolution. In this work, by introducing a sandwiched thermal shrink polymer film masking technique and a corresponding intermediate release agent, fine liquid alloy patterns were demonstrated by using a mechanical cutting plotter together with a common oven. The final resolution and shape of the mask could be tuned based on the anisotropy of the shrink polymer film and other operational parameters of the technique. After shrinkage, the width of the patterned liquid alloy lines and space in-between could be tuned to less than one third of the original cut pattern, to about 35 and 60 μm, respectively, according to requirements. To better predict the final structure, several parameters were investigated experimentally and numerically. Finally, a liquid alloy strain sensor and three-dimensional conformal masking were demonstrated, showing the potential of the developed technique.

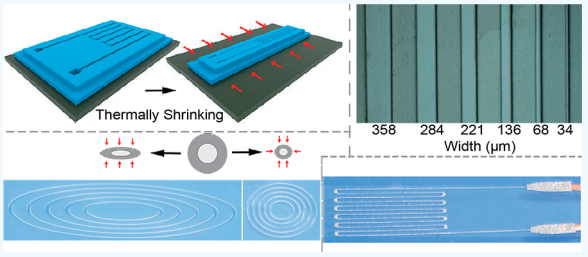

KEYWORDS: *masking, shrink film, resolution tuning, 3D conformal masking, liquid alloy patterning*

1. INTRODUCTION

With its potential to seamlessly integrate into the next generation of man−machine interfaces, stretchable electronics based on elastomers has drawn strong attention from various fields like epidermal electronics,[1,2] soft robotics,[3,4] microelectromechanical systems,[5,6] and medical diagnostics.[7,8] This is due to its attractive merits in being lightweight and compact while having abundant functions, at the same time as being compliant to complex and dynamic surfaces. Being intrinsically stretchable, liquid-alloy-based stretchable electronics[9−11] represent one alternative to permanently overcome the limitations of stretchability and long-term durability of rigid conductive materials. Numerous patterning techniques[12−14] have been developed to obtain high quality liquid alloy circuits for stretchable electronics, meeting the challenge from the extremely high surface energy of liquid alloys. Masking/stenciling is a ubiquitous tool to pattern or print electronic circuits, through which material can be deposited selectively. In particular, masked liquid alloy patterning[15−18] is one of the most promising techniques for scalable patterning of liquid-alloy-based stretchable electronics. However, high-resolution patterning is still challenging in practice and often constrained by the mask.

Traditionally, masks/stencils can be made by various lithographic techniques,[18−20] such as photolithography, electron beam, or X-ray lithography, which could achieve nanoscale resolution. These masks are often made by using a complex process with support from dedicated infrastructure. With the rapid development of lasers, selectively ablating materials such as a polymer or thin metal film, UV laser engraving[21] has become an effective and environmentally friendly tool to pattern a mask with a resolution in the micrometer scale. However, the necessary equipment for these techniques is expensive and not accessible for the majority of researchers. Being low-cost and highly accessible, mechanical cutting[12,16] is an excellent alternative candidate to making a stencil mask. However, due to the limited resolution, its processed mask is not so useful to many applications in stretchable electronics.

With the relaxing of the polymer chain, shrink polymer film can shrink to a certain ratio after heating. During manufacturing, the original entangled polymer chains has been orientated stretched.[22] With heating, the polymer chains reorganized to their original random pattern. The degree of shrinking is approximately equal to the stretch ratio of the orientation process. Previously, the shrink polymer has been

Received: October 11, 2018
Accepted: December 3, 2018
Published: December 3, 2018

DOI: 10.1021/acsapm.8b00010
ACS Appl. Polym. Mater. 2019, 1, 145−151

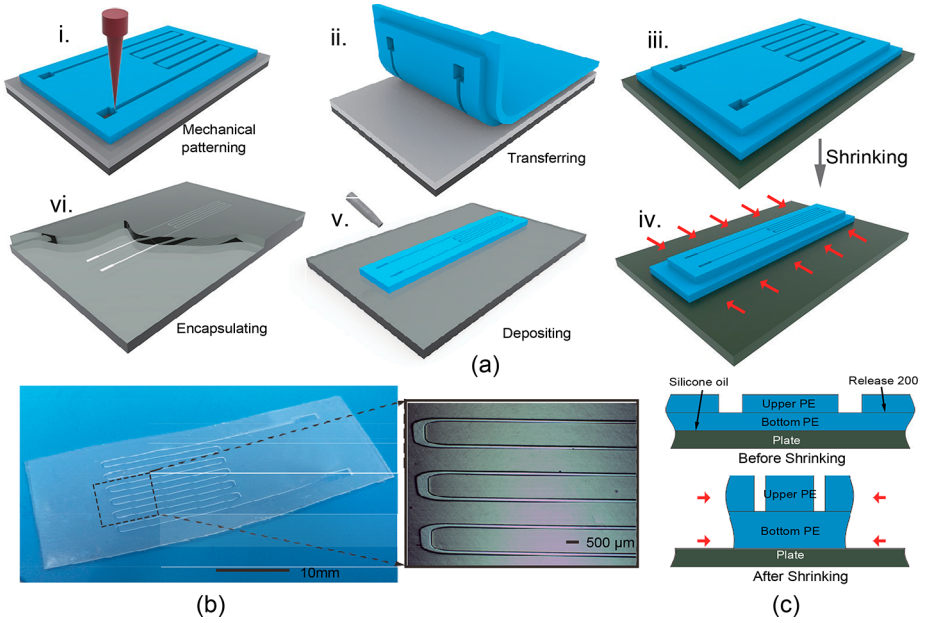

Figure 1. Illustration of the fabricating process of a strain sensor. (a) (i) The PE film is placed on a PDMS surface and then mechanically patterned by a cutter plotter. (ii) This original mask laminated with another layer of PE film are peeled off from the PDMS. (iii) The double layers of PE films were transferred onto an aluminum plate (iv) and uniaxially shrunk in an oven. The red arrows indicate the contracting direction. (v) The shrunk mask is transferred onto a soft substrate and sprayed over with liquid alloy. The mask is removed, producing the liquid alloy pattern of the strain sensor. (vi) Finally, the strain sensor is encapsulated. (b) Photo of the shrunk mask. (c) A comparison of a cross-section before and after shrinking.

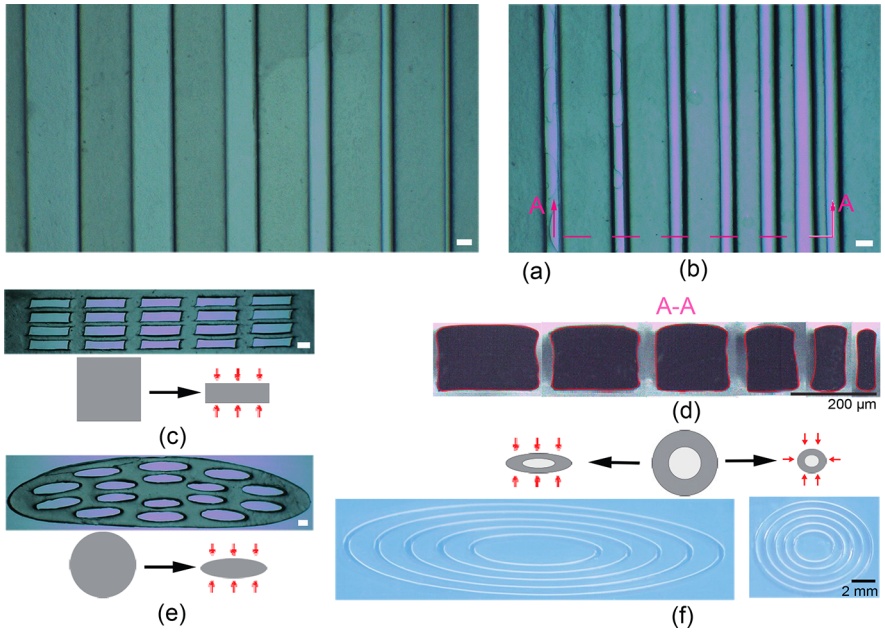

Figure 2. Shrunken PE masks. The unindicated scale bars mark 100 μm, and the red arrows indicate the contract direction. (a) The widths of channel are 34, 68, 136, 221, 284, and 358 μm, shrunk from the original 100, 200, 400, 600, 800, and 1000 μm, respectively. (b) The spaces are 60, 113, 173, 240, 298, and 349 μm, shrunk from the original 200, 400, 600, 800, 1000, and 1200 μm, respectively. Examples of the formation of matrix with rectangles (c) and ellipses (e) are shown in the diagram below. (d) The cross-section of A-A in (b). (f) Shrink masks from the same pattern but of different shrinkage anisotropy.

used to fabricate high aspect ratio structures[23−25] in microstructure molding, where the original shapes are directly etched[23] or deposited on films,[24] hence achieving smaller structures with higher aspect ratios after shrinking. Moreover, shrink polymer also was used to fabricate chips by stacking layers of patterned films.[26−30] After shrinking, a miniaturized version of microfluidic chip with high aspect ratio channel was obtained. However, all of these techniques focused on microstructures with high aspect ratios instead of exploring masking/stenciling resolution or shape tunability. By introducing shrink polymer film masking, the mask resolution could be tuned in some range towards higher resolution so that it becomes sufficient for more applications in stretchable electronics. With different pre-stretched methods and parameters in manufacturing, the shrink polymer film could shrink uniaxially or biaxially with different shrink ratios. In addition,

DOI: 10.1021/acsapm.8b00010
ACS Appl. Polym. Mater. 2019, 1, 145−151

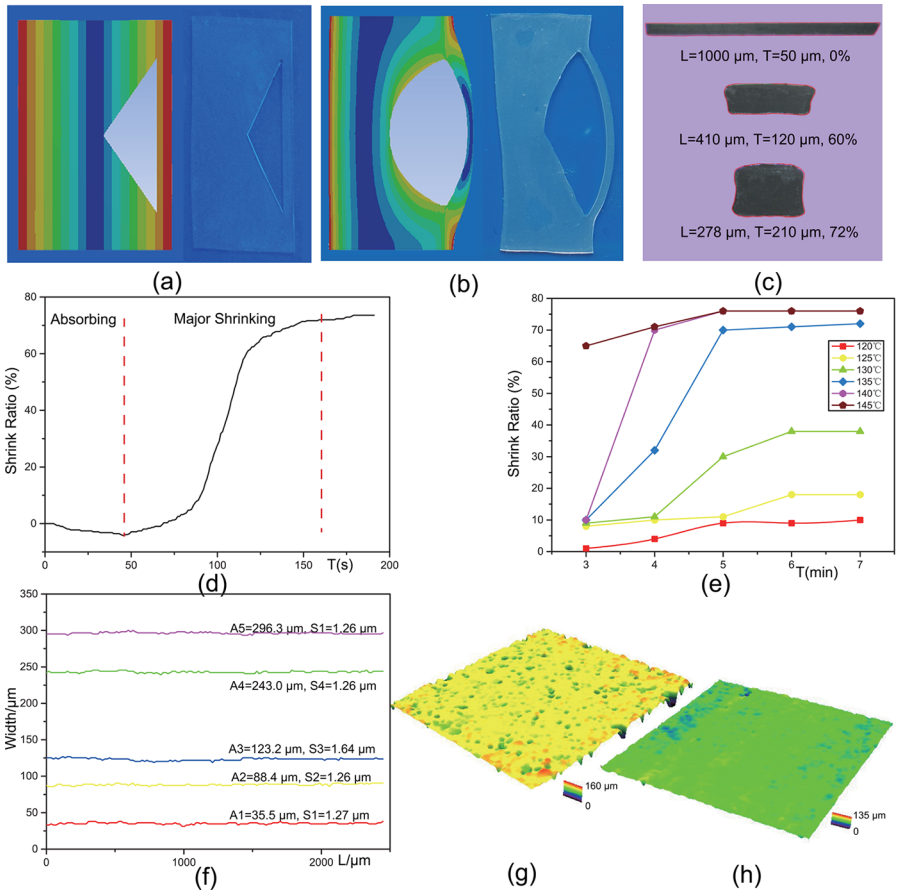

Figure 3. Analysis of the shrinking mechanism. The comparison of shrunk masks with (a) and without (b) double layer configuration of PE film, shrinking from the same original. (c) The cross-section from an original sized, 60% shrink, and 72% shrink PE film with corresponding thickness (*L* for length and *T* for thickness). When the film shrinks, it also rises in height, and the shape of its sidewall shifts. (d) Shrink ratio versus time. (e) Shrink ratio versus time and temperature. (f) Width variation of the channel (*A* for average and *S* for standard deviation). The roughness of original (g) and shrunken (h) surface of PE film.

the shrink ratio could be precisely controlled by adjusting the processing parameters in shrinking, including temperature and time, which allow the mask to obtain a variety of results. Moreover, due to fluidity in melting state, a planar mask could reflow and adapt to three-dimensional (3D) complex surfaces after shrinking and hence serve a 3D conformal mask. Polyethylene (PE) shrink polymer film is commonly used for packaging applications in the market. With features such as being soft, easy to process, and available in various thicknesses, it is well-suited as a stencil mask for depositing atomized liquid alloy, various inks, prepolymers, or paints.

By introducing a two-layer structure of thermal shrink polymer films with an intermediate release agent, a simple masking technique (Figure 1a) was developed to control and tune the resolution and shape of shadow mask for liquid alloy deposition. An original pattern was made by a mechanical cutting plotter on a thermal shrink film, and then was laminated on another layer of unpatterned shrink film with a thin layer of release agent. After shrinking the film in an oven, a mask with reduced dimensions was obtained and could be transferred onto a substrate for subsequent atomizing and deposition of the liquid alloy. To guide practical operations, adjustable parameters were studied more in detail. Finally, planar and 3D masks and their corresponding patterned circuits were fabricated to display the possibilities in application of this technique, where a strain sensor and a tactile sensor were demonstrated.

2. RESULTS AND DISCUSSION

Figure 1b exhibits a strain sensor mask with a serpentine pattern, and the diagram in Figure 1c displays the shrinking process. The dimension of whole film and its pattern were homogeneously reduced.

As shown in Figures 2a and b, the width of the open channels and the PE lines in-between could be as fine as 35 and 60 μm, respectively. Due to the low adhesion between the PE film and the PDMS below, the cutting plotter produced channel width, and PE lines were limited to approximately 100 and 200 μm, respectively. Furthermore, the PE structures were influenced by the increased aspect ratio of the cross-section when shrinking.

Figures 2c and e exhibit an anisotropic shrinking behavior of the uniaxial shrink film. Before shrinking, the original patterns were of squares and circles, but after uniaxial shrinkage of about 70%, the shrinking generated rectangles and ellipses.

When using a single layer of patterned PE film, the thermal induced shrinking force is rather weak compared to the friction between the film and the aluminum plate. If the patterned mask is complex with non-uniform distributed fragile structures or narrow lines, it will shrink non-uniformly and result in a distorted, or even broken, pattern. To address this

DOI: 10.1021/acsapm.8b00010
ACS Appl. Polym. Mater. 2019, 1, 145−151

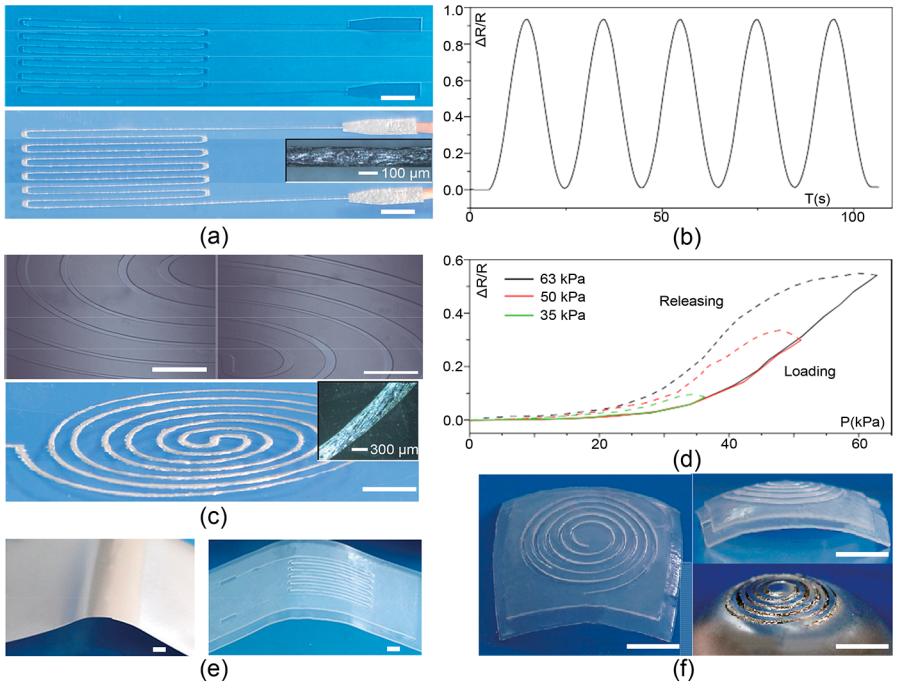

Figure 4. Shrunken PE masks and their respective sensors. The scale bars mark 5 mm. (a) Shrunken PE mask and deposited strain sensor, the inset is the partial micrograph of the circuit. (b) The resistance change of the strain sensor versus time. (c) A spiral tactile sensor (middle) deposited by a mask (top) shrunk from native circular-spiral (the inset is partial micrograph of the circuit), and (d) its response to different maximum pressures (35, 50, and 63 kPa), solid line and dashed line are loading and releasing of pressure. (e) Cylindrically curved mask (right), formed on a curved steel sheet (left). (f) A hemispherical spiral mask formed on a steel hemisphere and its deposited circuit on a PDMS hemisphere.

issue, the patterned PE film was stacked on top of an unpatterned PE film in the same shrinking orientation. To further improve uniformity, silicone oil was dripped on the aluminum plate to reduce the friction between the bottom PE film and aluminum plate. The bottom film shrunk in the same way as the upper film, which enabled the upper patterned film in maintaining a uniform shrinkage without distorting its patterns. Also, the bottom film acted as a buffer that reduced the friction to the aluminum plate below. Figure 2f shows a mask with isolated patterns. By adhering the patterned film to the unpatterned PE film below, it was possible to maintain the structure during shrinking, both in dimension control and in keeping the relative positions of isolated parts.

A more detailed comparison between shrinkage with and without the intermediate blank PE film was performed experimentally and numerically. A representative structure is shown in Figures 3a and b. A rectangular film was patterned with a triangular opening and a narrow stripe on its right. A simple approximation from mechanics is that without the underlaying PE film, due to the small inertia of the stripe, the narrow stripe was dragged from two ends with the major force from the major body. Hence, with its low Young's modulus and yielding point, the pattern deformed, as seen in Figure 3b. With a set shrink ratio, a static structure analysis (Supporting Information S1 and Figure S1) was performed to observe the deforming trend, left column in Figures 3a and b, that can be used as an approximate guideline of the shrinking behavior.

The thin layer of the Release 200 used to laminate the two layers of PE films served both as an adhesive and a separator in different situations. It resulted in that during the laminated state, the agent bonded the two layers to assist the film transfer and provided a uniform contracting movement when shrinking. Meanwhile, it also hindered a permanent bonding of the two layers during the high temperature shrinking. To note, the support plate also affected the mask quality: when quartz glass was used to replace the aluminum plate, a distorted pattern was found. This phenomenon is due to the low thermal conductivity of glass, as shown in Supporting Information S2 and Figure S2.

As a stencil mask, the shape of its side walls strongly impacts the final pattern. Figure 3c displays the shapes of the cross-section with increasing shrink ratio: directly from the cutting plotter, to being shrunken 60 and 72%. At 60%, the shape was similar to the original although thicker, but at 72%, the side wall became a concave arc. Probably, when cooling from melting to solid state at a thickness of 210 μm, it was thick enough to allow the cooling gradient over the film thickness to produce a contraction of the middle section. By tuning the process parameters, a certain wall shape could be designed for a particular purpose. For example, the shape of the side wall impacts liquid alloy deposition, cf. Supporting Information S3 and Figure S3. A side wall with negative slope better isolates the liquid alloy on the substrate from that on the mask than what the arc shaped side wall does. Furthermore, such features could be used to mold channels with cross-section of trapezoidal or round walls, which in micrometer scale often is difficult to obtain.

To conformally attach to substrates, the mask should be kept flexible enough. If the mask is too thick, it becomes too stiff to transfer or delaminate, which leads to low quality liquid alloy pattern. In this work, at 72% shrinkage it was 210 μm thick, which was the limit for us before it became too thick and too rigid for a good mask. Therefore, the initial thickness should be considered with the shrink ratio before processing.

In practice, by choosing different shrink films, its features can be adjusted for specific purposes, e.g., thickness, uniaxial or

DOI: 10.1021/acsapm.8b00010
ACS Appl. Polym. Mater. 2019, 1, 145−151

biaxial shrinking direction, and shrinkage ratio. Among them, shrinking mode is a decisive feature. It determines the basic pattern traction modes and hence the final pattern after shrinking. A proper selection will not only enable new patterns difficult to obtain from the cutting plotter (Figure 2f) but also reduce the risk of damaging the mask during the shrinking. For example, a strain sensor usually only requires high resolution in one direction, so a uniaxial shrink film was selected to avoid the shrinking movement in other direction. One advantage is that the thickness increase of a uniaxial shrunk mask is half of that of a biaxial, which provides higher flexibility. Meanwhile, a tactile sensor requires high resolution in all directions in the plane. Hence, a biaxial shrink film was used for this purpose, as shown in Figure 2f (it shrunk about 44% in one direction and 36% orthogonally to that).

Also, it is possible to tune the thickness by controlling temperature and time during the shrinking process. Figure 3d describes the relation between the time and shrinkage at a set temperature (140 °C) in the oven. Initially, there was a small expansion due to thermal expansion. After that, the shrinking occurred exponentially with time. In this period, we observed that nearly all stored pre-stress was released. Due to the thermal inertia, contracting still continued after taking the film out from the oven, and the final shrink ratio of the cooled sample was measured to assist in controlling the thickness, Figure 3e. It showed that the relation of shrinkage versus time and temperature, and the final shrink ratio was primarily determined by temperature. With increasing temperature, the final shrink ratio became higher until it stabilized at 145 °C. In our process, the total shrinking time is different because of different coverage conditions (Supporting Information S4) but the major shrinking processes are done in about 1 min.

To investigate the precision of the mask, Figure 3f presents the width average and standard deviation of several channels from the mask. The variations were partly caused by weak adhesion of Release 200, which led to a slip in transferring or shrinking. This phenomenon is increased by a high aspect ratio of the pattern. As shown in Figure 2d, the rightmost cross-section is 60 μm in width and 210 μm in height, having an aspect ratio of 3.5, which may cause falling of the PE lines during the shrinking process. The roughness of surface may have contributed to this failure mechanism. Figure 3g exhibits the morphology and roughness before and after shrinkage, where many micropits on the PE film surface disappeared after shrinking, and the area roughness was reduced from 8 to 3 μm. The morphology change may be a reason for the slight waggling of the upper layer of the PE film, which in turn may have induced a variation of the side wall inclination.

Figure 4a displays a packaged strain sensor that was patterned by this technique. The original width of pattern was 200 μm, and it was improved to about 100 μm after uniaxial shrinkage. The performance of resistive response to stretching is shown in Figure 4b. A slightly elliptical spiral circuit was also deposited, Figure 4c, using a uniaxial shrink film from a circular spiral cutter plotter pattern, and the resistance change versus different loading and releasing pressure was measured by a digital multimeter (Figure 4d), demonstrating a rudimentary tactile sensor. Due to the hysteresis of the elastomer, the releasing process showed a noticeable hysteresis. The hysteresis was varied with different maximum pressure and compression rates.[10]

Finally, to further explore the potential of this technique in masking, a cylindrical conformal mask was fabricated from an original planar pattern on PE film, Figure 4e. It was then conformally shaped by pressurizing with a cylindrical steel sheet. Moreover, the spatial mask in Figure 4f was fabricated with a slightly modified process (Supporting Information S5 and Figure S4). The whole structure was entirely wrapped by another layer of PE film, which generated an even force to push the mask shrinking toward the surface of the steel hemisphere. Along with this spatial mask, a spiral circuit was deposited on a PDMS hemisphere. In the future, by establishing a platform that could uniformly add pneumatic or hydraulic pressure to the film surface, with a sufficient flexibility it should be possible to fabricate conformal masks for more complex surfaces.

3. SUMMARY

By introducing a thermal shrink polymer film, this technique provides a facile way to fabricate a mask with tunable resolution and shape. With proper tuning, it can achieve a relatively high-resolution of mask from an initial mechanically produced low-resolution, which is a universal tool in micropatterning. The sandwiched structure, consisting of a double layer films and interface design, that enables a final high-quality mask, has been studied experimentally and numerically. Moreover, with the characteristic of shrink polymer material, adjustable parameters like shrink ratio and anisotropy, and heating time and temperature, have been analyzed to better tune the resolution and shape of a mask. Finally, a few sensors, and hemispherically and cylindrically conformal masks, have been fabricated to demonstrate the capability of this technique.

4. EXPERIMENTAL SECTION

4.1. Fabrication of Shrunk Mask. A layer of PDMS (Sylgard 184, Dow Corning; 10:1 base-to-curing agent) was poured on a PET foil (100 μm thick) and flattened by an applicator (50 μm). After curing in an oven (UF55, Memmert, Germany) at 75 °C for about 5 min, a PE shrink film (60 μm) was smoothly attached on the PDMS surface, and bubbles were removed with a plastic scraper.

With a stiffer but flexible support of the PET foil, the PE film was patterned by a commercial mechanical cutting plotter (CE6000-40, GRAPHTEC). After creating the mask pattern by removing the unwanted PE material, a thin layer of the agent Release 200 (Smooth-On, United States) was sprayed on this original mask. After that, an unpatterned PE film was attached to the surface with the same shrink direction. Both layers were together gently peeled off the PDMS and placed onto a flat aluminum plate (1 mm in thickness) with a thin layer of silicone oil in-between. After being moved into a closed glass container, the plate with its double layer PE films was moved into an oven (DHG-9023A, Bluepard) at 140 °C for about 10 min (prior to that, the oven platform should be precisely levelled). Finally, after taking the plate out of the oven and cooling it to room temperature, a shrunk mask was obtained.

4.2. Liquid Alloy Patterning. After cleaning, the mask was transferred onto a semi-cured PDMS surface for depositing. The gallium-based liquid alloy Galinstan (68.5% Ga, 21.5% In, 10% Sn, Gerather Medical AG, Germany) was atomized and sprayed on the mask by a manual airbrush (Meectools, Jula, Sweden) coupled to a pressure regulator (ML-5000XII, Musashi, Japan). After peeling off the mask from the substrate with its liquid alloy, the circuit was patterned. Copper foil electrodes were brought into contact with the liquid alloy to interconnect with an external circuit. The final circuit or sensor was encapsulated by pouring over and curing another layer of PDMS thereon.

4.3. Characterization of the Mask and Demonstration. The micrographs were taken by an optical microscope (BA310MET-T, Motic, China) with a CCD camera, and the dimension of width and space was measured by a standard scale. In Figure 3d, the curve was

DOI: 10.1021/acsapm.8b00010
ACS Appl. Polym. Mater. 2019, 1, 145−151

drawn by measuring the distance of two parallel lines on PE film at 140 °C extracted by a MatLab program from a video of a shrinking process (Supporting Information S6 and Figure S5). To test the performance of the strain sensor, its two ends were fixated on a dynamic tensile system (E1000, Instron, United States). During stretching and releasing of this system, the resistance change of the sensor was recorded by a Data Acquisition/Switch Unit (34972A, KeySight Technologies, United States). The point pressure when testing the tactile sensor was provided by a stepper motor and quantified by a manometer. The roughness of the surface was acquired using a digital microscope (DSX510, OLYMPUS, Japan).

■ ASSOCIATED CONTENT

Supporting Information

The Supporting Information is available free of charge on the ACS Publications website at DOI: 10.1021/acsapm.8b00010.

S1: snapshots of simulation results (Figure S1); S2: illustration of importance of plate material (Figure S2); S3: illustration of importance of negative slope of cross-section (Figure S3); S4: different coverage conditions; S5: three- dimensional conformal mask fabrication (Figure S4); S6: illustration of Figure 3d (Figure S5) (PDF)

■ AUTHOR INFORMATION

Corresponding Author

*E-mail: Zhigang.Wu@angstrom.uu.se or zgwu@hust.edu.cn.

ORCID

Chuanfei Guo: 0000-0003-4513-3117

Zhigang Wu: 0000-0002-3719-406X

Author Contributions

⊥B.W. and W.X. contributed equally.

Author Contributions

Z.W. and B.W. conceived the concept and designed the experiments. B.W. and W.X. conducted the experimental and simulation works. All authors contributed to data analysis and manuscript preparation.

Notes

The authors declare no competing financial interest.

■ ACKNOWLEDGMENTS

We acknowledge support from National Natural Science Foundation of China (Grants U1613204 and 51575216) and Pearl River Talents Recruitment Program (Grant 2016ZT06G587). C.G. and Z.W. thank the Chinese central government for support through its Thousand Youth Talents program.

■ REFERENCES

(1) Rogers, J. A.; Someya, T.; Huang, Y. Materials and Mechanics for Stretchable Electronics. *Science* **2010**, *327*, 1603−1607.

(2) Kim, D. H.; Lu, N.; Ma, R.; Kim, Y. S.; Kim, R. H.; Wang, S.; Wu, J.; Won, S. M.; Tao, H.; Islam, A.; Yu, K. J.; Kim, T.; Chowdhury, R.; Ying, M.; Xu, L.; Li, M.; Chung, H. J.; Keum, H.; McCormick, M.; Liu, P.; Zhang, Y. W.; Omenetto, F. G.; Huang, Y.; Coleman, T.; Rogers, J. A. Epidermal Electronics. *Science* **2011**, *333*, 838−843.

(3) Kim, S.; Laschi, C.; Trimmer, B. Soft Robotics: A Bioinsipred Evolution in Robotics. *Trends Biotechnol.* **2013**, *31*, 287−294.

(4) Rus, D.; Tolley, M.T. Design, Fabrication and Control of Soft Robots. *Nature* **2015**, *521*, 467−475.

(5) Park, S. I.; Xiong, Y.; Kim, R. H.; Elvikis, P.; Meitl, M.; Kim, D. H.; Wu, J.; Yoon, J.; Yu, C. J.; Liu, Z.; Huang, Y.; Hwang, K.; Ferreira, P.; Li, X.; Choquette, K.; Rogers, J. A. Printed Assemblies of Inorganic Light-Emitting Diodes for Deformable and Semitransparent Displays. *Science* **2009**, *325*, 977−981.

(6) Kim, D. H.; Ahn, J. H.; Choi, W. M.; Kim, H. S.; Kim, T. H.; Song, J.; Huang, Y. Y.; Liu, Z.; Lu, C.; Rogers, J. A. Stretchable and Foldable Silicon Integrated Circuits. *Science* **2008**, *320*, 507−511.

(7) El-Ali, J.; Sorger, P. K.; Jensen, K. F. Cells on Chips. *Nature* **2006**, *442*, 403−411.

(8) Wu, Z. G.; Willing, B.; Bjerketorp, J.; Jansson, J. K.; Hjort, K. Soft Inertial Inertial Microfluidics for High Trhoughput Separation of Bacteria from Human Blood Cells. *Lab Chip* **2009**, *9*, 1193−1199.

(9) Cheng, S.; Rydberg, A.; Hjort, K.; Wu, Z. G. Liquid Metal Stretchable Unbalanced Loop Antenna. *Appl. Phys. Lett.* **2009**, *94*, 144103.

(10) Park, Y. L.; Chen, B. R.; Wood, R. J. Design and Fabrication of Soft Artificial Skin Using Embedded Microchannels and Liquid Conductors. *IEEE Sens. J.* **2012**, *12*, 2711−2718.

(11) Palleau, E.; Reece, S.; Desai, S. C.; Smith, M. E.; Dickey, M. D. Self-Healing Stretchable Wires for Reconfigurable Circuit Wiring and 3D Microfluidics. *Adv. Mater.* **2013**, *25*, 1589−1592.

(12) Jeong, S. H.; Hagman, A.; Hjort, K.; Jobs, M.; Sundqvist, J.; Wu, Z. G. Liquid Alloy Printing of Microfluidic Stretchable Electronics. *Lab Chip* **2012**, *12*, 4657−4664.

(13) Zheng, Y.; He, Z.; Gao, Y.; Liu, J. Direct Desktop Printed-Circuits-on-Paper Flexible Electronics. *Sci. Rep.* **2013**, *3*, 1786.

(14) Lu, T.; Finkenauer, L.; Wissman, J.; Majidi, C. Rapid Prototyping for Soft-Matter Electronics. *Adv. Funct. Mater.* **2014**, *24*, 3351−3356.

(15) Kramer, R. K.; Majidi, C.; Wood, R. J. Masked Deposition of Gallium-Indium Alloys for Liquid-Embedded Elastomer Conductors. *Adv. Funct. Mater.* **2013**, *23*, 5292−5296.

(16) Jeong, S. H.; Hjort, K.; Wu, Z. G. Tape Transfer Atomization Patterning of Liquid Alloys for Microfluidic Stretchable Wireless Power Transfer. *Sci. Rep.* **2015**, *5*, 8419.

(17) Sahlberg, A.; Nilsson, F.; Berglund, A.; Nguyen, H.; Hjort, K.; Jeong, S. H. High-Resolution Liquid Alloy Patterning for Small Stretchable Strain Sensor Arrays. *Adv. Mater. Technol.* **2018**, *3*, 1700330.

(18) Park, C. W.; Moon, Y. G.; Seong, H.; Jung, S. W.; Oh, J. Y.; Na, B. S.; Park, N. M.; Lee, S. S.; Im, S. G.; Koo, J. B. Photolithography-Based Patterning of Liquid Metal Interconnects for Monolithically Integrated Stretchable Circuits. *ACS Appl. Mater. Interfaces* **2016**, *8*, 15459−15465.

(19) Zhou, Y. X.; Hone, J.; Smith, W. F.; Johnson, A. T. Simple Fabrication of Molecular Circuits by Shadow Mask Evaporation. *Nano Lett.* **2003**, *3*, 1371−1374.

(20) Brambley, D.; Martin, B.; Prewett, P. D. Microlithography: An Overview. *Adv. Mater. Opt. Electron.* **1994**, *4*, 55−74.

(21) Peng, P.; Wu, K.; Lv, L. X.; Guo, C. F.; Wu, Z. G. One-Step Selective Adhesive Transfer Printing for Scalable Fabrication of Stretchable Electronics. *Adv. Mater. Technol.* **2018**, *3*, 1700264.

(22) Hidber, P. C.; Nealey, P. F.; Helbig, W.; Whitesides, G. M. New Strategy for Controlling the Size and Shape of Metallic Features Formed by Electroless Deposition of Copper: Microcontact Printing of Catalysts on Oriented Polymers, Followed by Thermal Shrinkage. *Langmuir* **1996**, *12*, 5209−5215.

(23) Zhao, X. M.; Xia, Y. N.; Qin, D.; Whitesides, G. M. Fabrication of Polymeric Microstructures with High Aspect Ratios Using Shrinkable Polystyrene Films. *Adv. Mater.* **1997**, *9*, 251−254.

(24) Grimes, A.; Breslauer, D. N.; Long, M.; Pegan, J.; Lee, L. P.; Khine, M. Shrinky-Dink Microfluidics: Rapid Generation of Deep and Rounded- Patterns. *Lab Chip* **2008**, *8*, 170−172.

(25) Nguyen, D.; Taylor, D.; Qian, K.; Norouzi, N.; Rasmussen, J.; Botzet, S.; Lehmann, M.; Halverson, K.; Khine, M. Better Shrinkage than Shrinky-Dinks. *Lab Chip* **2010**, *10*, 1623−1626.

(26) Chen, C. S.; Breslauer, D. N.; Luna, J. I.; Grimes, A.; Chin, W. C.; Lee, L. P.; Khine, M. Shrinky-Dink Microfluidics: 3D Polystyrene Chips. *Lab Chip* **2008**, *8*, 622−624.

(27) Sollier, K.; Mandon, C. A.; Heyries, K. A.; Blum, L. J.; Marquette, C. A. "Print-N- Shrink" Technology for the Rapid

Production of Microfluidic Chips and Protein Microarrays. *Lab Chip* **2009**, *9*, 3489−3494.
(28) Long, M.; Sprague, M. A.; Grimes, A. A.; Rich, B. D.; Khine, M. A Simple Three-Dimensional Vortex Micromixer. *Appl. Phys. Lett.* **2009**, *94*, 133501.
(29) Taylor, D.; Dyer, D.; Lew, V.; Khine, M. Shrink Film Patterning by Craft Cutter: Complete Plastic Chips with High Resolution/High-Aspect Ratio Channel. *Lab Chip* **2010**, *10*, 2472−2475.
(30) Nguyen, D.; McLane, J.; Lew, V.; Pegan, J.; Khine, M. Shrink-Film Microfluidic Education Modules: Complete Devices within Minutes. *Biomicrofluidics* **2011**, *5*, 022209.

DOI: 10.1021/acsapm.8b00010
ACS Appl. Polym. Mater. 2019, 1, 145−151